Cent. Eur. J. Phys. • 10(4) • 2012 • 779-788
DOI: 10.2478/s11534-012-0051-x

VERSITA

Central European Journal of **Physics**

Effect of kinesin velocity distribution on slow axonal transport

Research Article

Andrey V. Kuznetsov[1]*

1 *Dept. of Mechanical and Aerospace Engineering, North Carolina State University, Campus Box 7910, Raleigh, NC 27695-7910, USA*

Received 05 December 2011; accepted 21 March 2012

Abstract: The goal of this paper is to investigate the effect that a distribution of kinesin motor velocities could have on cytoskeletal element (CE) concentration waves in slow axonal transport. Previous models of slow axonal transport based on the stop-and-go hypothesis (P. Jung, A. Brown, Modeling the slowing of neurofilament transport along the mouse sciatic nerve, Physical Biology 6 (2009) 046002) assumed that in the anterograde running state all CEs move with one and the same velocity as they are propelled by kinesin motors. This paper extends the aforementioned theoretical approach by allowing for a distribution of kinesin motor velocities; the distribution is described by a probability density function (PDF). For a two kinetic state model (that accounts for the pausing and running populations of CEs) an analytical solution describing the propagation of the CE concentration wave is derived. Published experimental data are used to obtain an analytical expression for the PDF characterizing the kinesin velocity distribution; this analytical expression is then utilized as an input for computations. It is demonstrated that accounting for the kinesin velocity distribution increases the rate of spreading of the CE concentration waves, which is a significant improvement in the two kinetic state model.

PACS (2008): 87.16.-b

Keywords: slow axonal transport • stop-and-go hypothesis • neurons • molecular motors • exact solution

1. Introduction

Neurons, the specialized cells of the nervous system, have very long processes, axons and dendrites; axons transmit signals while dendrites receive signals. Support of signal-transmitting function of axons and signal-receiving function of dendrites requires various proteins. Most chemical synthesis occurs in the neuron body; protein synthesis includes such steps as production of messenger RNAs (mRNAs), mRNA transport and translation into proteins that occurs in ribosomes, protein processing, packaging, and trafficking [1]. Other components that are required for axon and dendrite functioning include cytoskeletal elements, which are building blocks of axonal and dendritic cytoskeletons. Synthesized particles must be transported to particular locations in the axons and dendrites where they are needed, and used components must be returned to the cell body for reprocessing. Explaining how this is done in axons is especially challenging because axons can be very long (in a human body they can be up to 1 m in

*E-mail: avkuznet@eos.ncsu.edu

length) [2].

Depending on its velocity, anterograde axonal transport is divided into three categories: fast axonal transport, component B of slow axonal transport, and component A of slow axonal transport. In fast axonal transport cargos move with an average velocity of 1–5 μm/s, in component B of slow axonal transport they move with the average velocity of 0.02–0.09 μm/s, and in component A they move with an average velocity of 0.002–0.01 μm/s. Retrograde axonal transport occurs only at a "fast" velocity of 1–5 μm/s. The particular mode of transport typically depends on the type of cargo; for example, organelles and vesicles are transported by fast axonal transport while neurofilaments (NFs) are transported by component A of slow axonal transport [3–8].

Axonal transport is powered by two types of molecular motors, kinesins and dyneins. In axons kinesins are responsible for anterograde motion while dyneins are responsible for retrograde motion. Both of these motor types walk along microtubules (MTs) and extract energy from ATP hydrolysis. Since velocity of fast anterograde axonal transport corresponds to velocity of kinesins, it is believed that in this mode cargos are directly pulled by kinesin motors. Likewise, in retrograde axonal transport cargos are directly pulled by dynein motors. There is extensive evidence that cargos in slow axonal transport are also moved by kinesin and dynein motors, but in this case motors do not pull the cargos continuously; periods of rapid motion are followed by pauses, which can be short (where motors remain attached to MTs) or long (where motors detach from MTs) [1, 9–14, 16–18]. By considering a change in the motor "duty cycle" (the ratio of the cargo residence time in the running state to that in the pausing state) one can explain how different velocities observed in slow axonal transport can be caused by the action of the same molecular motors that are responsible for fast axonal transport. The above explanation is summarized by the stop-and-go hypothesis [19–22], which states that cargo pausing is the main reason explaining why the average cargo velocity in slow axonal transport is many times (often by a factor of 100) smaller than the velocity of motors that propel this motion. Utilizing the stop-and-go hypothesis, Jung and Brown [23] developed several models of various complexities that simulate slow axonal transport of NFs in axons. The basic model (the one utilized in the present research) accounts only for two kinetic states of NFs, pausing and running. Numerical and perturbation solutions of equations developed in [23] were reported in [24–30].

The purpose of this paper is, building on analytical techniques developed in [31] and [32], to investigate the effect of kinesin motor velocity distribution on slow axonal transport. As demonstrated in [31] and [32], the major difficulty of the basic two kinetic state model of Jung and Brown [23] is insufficient rate of spreading of the concentration wave, which is much less than experimentally reported [33]. One possible improvement of the model is accounting for the kinesin velocity distribution. This paper investigates how accounting for this effect impacts the solution behavior and, in particular, the rate of spreading of the concentration wave.

2. Governing equations

A schematic diagram showing a neuron, an axon, the injection point of the CEs, and the coordinate system is displayed in Fig. 1 (a), Fig. 1 (b) depicts a kinetic diagram showing two CE populations (pausing and running) and kinetic processes between them. It is assumed that the kinetic processes are described by first-order reactions. Fig. 1 (c) displays the initial condition. It is assumed that at $t^* = 0$ all injected CEs are in the running state, and that they initially form a uniform pulse of width x_c^*. The origination point of the coordinate system is located at the left-hand side of the initial pulse. Under these assumptions, the governing equations (which correspond to Eq. (7) in [23]) are

$$\frac{\partial n_0^*}{\partial t^*} = -\gamma_{01}^* n_0^* + \gamma_{10}^* n_1^* , \tag{1}$$

$$\frac{\partial n_1^*}{\partial t^*} = -v^* \frac{\partial n_1^*}{\partial x^*} + \gamma_{01}^* n_0^* - \gamma_{10}^* n_1^* , \tag{2}$$

where n_0^* is the linear number density of CEs (number of CEs per unit length of the axon) in the pausing state (particles/μm), n_1^* is the linear number density of CEs in the running state (particles/μm), γ_{01}^* is a first-order rate constant describing the probability of transition from the pausing to the running state (1/s), γ_{10}^* is a first-order rate constant describing the probability of transition from the running to the pausing state, see Fig. 1 (b), (1/s), v^* is the kinesin motor velocity, calculated excluding pauses (μm/s), x^* is the linear coordinate along the axon (μm), and t^* is the time (s). Asterisks denote dimensional variables.

From the kinetic diagram displayed in Fig. 1 (b) it is evident that for large t^* (when equilibrium is established), the residence time of a CE in the running state is proportional to γ_{01}^* and the residence time of a CE in the pausing state is proportional to γ_{10}^*. Since in the running state a CE moves with velocity v^* and in the pausing state a CE does not move, the average velocity of a CE for large t^* is $\overline{v^*} = v^* \frac{\gamma_{01}^*}{\gamma_{01}^* + \gamma_{10}^*}$.

Jung and Brown [23] also presented more sophisticated models that accounted for reversals from anterograde to

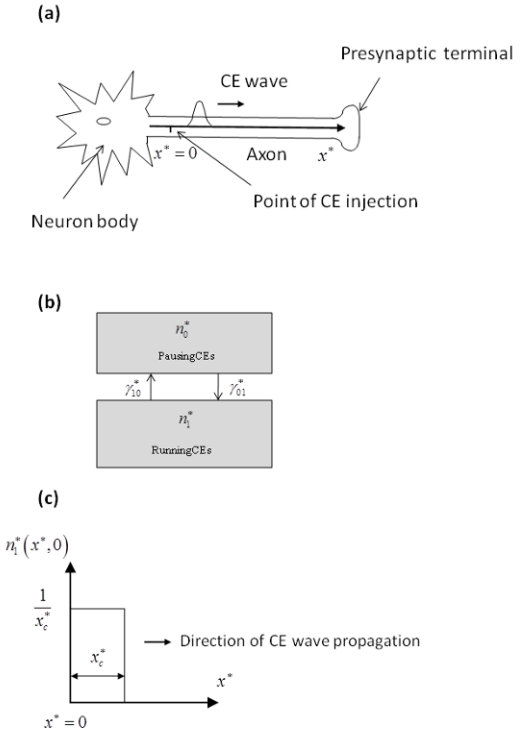

Figure 1. (a) Sketch of an axon and a coordinate system; (b) A diagram showing two populations of CEs (running and pausing) and kinetic processes between them; (c) A diagram illustrating the initial condition (when CEs have just been injected into the axon)

retrograde motion and vice versa, but the important features of the model of slow axonal transport based on the stop-and-go hypothesis can be captured by Eqs. (1) and (2).

The total linear number density of CEs (in the pausing and running states), which is the parameter accessible to experiments, is

$$n^*(x^*, t^*) = n_0^*(x^*, t^*) + n_1^*(x^*, t^*)\,. \tag{3}$$

Another way of interpreting the functions n_0^* and n_1^* (suggested in [23]) is to view these functions as the probability densities of finding a CE in the pausing and running states, respectively. The two approaches are identical because for an ensemble of independent CEs the concentration of CEs in a particular kinetic state is proportional to the probability of finding a CE in that kinetic state. Since the probability of finding a CE in one of the kinetic states somewhere in the axon is equal to 100%, n^* is normalized by the following condition:

$$\int_0^\infty n^*(x^*, t^*)dx^* = 1\,. \tag{4}$$

Since CEs in the motor-driven state are the only CEs that can move, the flux of CEs (particles/s) is given by

$$j^* = v^* n_1^*\,. \tag{5}$$

At $x^* = 0$ a no CE-flux condition is imposed. Eqs. (1) and (2) are thus solved subject to the following boundary condition:

$$n_1^*(0, t^*) = 0\,. \tag{6}$$

The dimensionless forms of Eqs. (1) and (2) are

$$\frac{\partial n_0}{\partial t} = -n_0 + \gamma_{10} n_1\,. \tag{7}$$

$$\frac{\partial n_1}{\partial t} = -\frac{\partial n_1}{\partial x} - \gamma_{10} n_1 + n_0\,. \tag{8}$$

where

$$n_0 = \frac{n_0^* v^*}{\gamma_{01}^*}\,,\quad n_1 = \frac{n_1^* v^*}{\gamma_{01}^*}\,,\quad t = t^* \gamma_{01}^*\,,$$
$$x = \frac{x^* \gamma_{01}^*}{v^*}\,,\quad \gamma_{10} = \frac{\gamma_{10}^*}{\gamma_{01}^*} \tag{9}$$

and the dimensionless total linear number density of CEs, $n = n_0 + n_1$ is defined as $\frac{n^* v^*}{\gamma_{01}^*}$. The dimensionless average velocity of a CE for large t, defined as $\overline{v} = \frac{\overline{v}^*}{v^*}$. is $\overline{v} = \frac{1}{1+\gamma_{10}}$. When CEs are injected, they are all initially assumed to be in the running state. It is also assumed that initially CEs form a uniform pulse confined between $0 \le x \le x_c$ with an amplitude of $\frac{1}{x_c}$ (where $x_c = \frac{x_c^* \gamma_{01}^*}{v^*}$), so that the condition $\int_0^\infty n(x, t)dx = 1$ is satisfied. Mathematically this initial condition can be described as follows:

$$n_0(x, 0) = 0\,, \tag{10}$$

$$n_1(x, 0) = \frac{1}{x_c}(H[x] - H[x - x_c])\,, \tag{11}$$

where H is the Heaviside step function.

The subsidiary equations are

$$s\overline{n_0} = -\overline{n_0} + \gamma_{10}\overline{n_1}\,, \tag{12}$$

$$s\overline{n_1} - \frac{1}{x_c}(H[x] - H[x - x_c]) = -\frac{\partial \overline{n_1}}{\partial x} - \gamma_{10}\overline{n_1} + \overline{n_0}\,. \tag{13}$$

Eqs. (12) and (13) are solved subject to the following boundary condition: $\overline{n_1}(0,s)=0$, which stems from Eq. (6). The solutions of the subsidiary equations are

$$\begin{aligned}\overline{n_0} =& \frac{\gamma_{10}(1-H[x-x_c])}{sx_c(1+s+\gamma_{10})} - e^{-sx}\frac{\gamma_{10}\exp[-\gamma_{10}x]}{sx_c(1+s+\gamma_{10})}\exp\left[\frac{\gamma_{10}x}{1+s}\right]\\ &+\exp[-s(x-x_c)]\frac{\gamma_{10}\exp[-\gamma_{10}(x-x_c)]H[x-x_c]}{sx_c(1+s+\gamma_{10})}\\ &\times\exp\left[\frac{\gamma_{10}(x-x_c)}{1+s}\right], \end{aligned} \tag{14}$$

$$\begin{aligned}\overline{n_1} =& -\frac{(1+s)(-1+H[x-x_c])}{sx_c(1+s+\gamma_{10})}\\ &- e^{-sx}\exp[-\gamma_{10}x]\frac{1+s}{sx_c(1+s+\gamma_{10})}\exp\left[\frac{\gamma_{10}x}{1+s}\right]\\ &+\exp[-s(x-x_c)]\exp[-\gamma_{10}(x-x_c)]\frac{(1+s)H[x-x_c]}{sx_c(1+s+\gamma_{10})}\\ &\times\exp\left[\frac{\gamma_{10}(x-x_c)}{1+s}\right], \end{aligned} \tag{15}$$

In calculating the inverse Laplace transforms of the right-hand sides of Eqs. (14) and (15) the use is made of the convolution integral (the superposition theorem) [34, 35] as well as of the property of the inverse Laplace transform that $L^{-1}\{\exp[-as]F(s)\}=f(t-a)H[t-a]$. The following solutions for the CE concentrations are obtained:

$$\begin{aligned} n_0(x,t) =& -\tfrac{\exp[-t(1+\gamma_{10})](-1+\exp[t(1+\gamma_{10})])\gamma_{10}(-1+H[x-x_c])}{x_c(1+\gamma_{10})}\\ &+\left\{-\tfrac{\exp[-(t-x)-t\gamma_{10}](-1+\exp[(t-x)(1+\gamma_{10})])\gamma_{10}}{x_c(1+\gamma_{10})}\right.\\ &-\int_0^{t-x}\tfrac{1}{x_c(1+\gamma_{10})}\exp[-(t-x-\tau)-(t-\tau)\gamma_{10}]\\ &\times(-1+\exp[(t-x-\tau)(1+\gamma_{10})])\gamma_{10}\exp[-\tau]\\ &\left.\times\tfrac{\sqrt{x\gamma_{10}}}{\sqrt{\tau}}I_1[2\sqrt{\tau x\gamma_{10}}]d\tau\right\}H[t-x]\\ &+\left\{\tfrac{\gamma_{10}}{x_c(1+\gamma_{10})}\exp[(-x+x_c)\gamma_{10}-(t-x+x_c)(1+\gamma_{10})]\right.\\ &\times(-1+\exp[(t-x+x_c)(1+\gamma_{10})])\\ &+\int_0^{t-x+x_c}\tfrac{\gamma_{10}}{x_c(1+\gamma_{10})}\exp[(-x+x_c)\gamma_{10}-(t-x+x_c-\tau)\\ &\times(1+\gamma_{10})](-1+\exp[(t-x+x_c-\tau)(1+\gamma_{10})])\\ &\left.\times\exp[-\tau]\tfrac{\sqrt{(x-x_c)\gamma_{10}}}{\sqrt{\tau}}I_1[2\sqrt{\tau(x-x_c)\gamma_{10}}]d\tau\right\}\\ &\times H[x-x_c]H[t-x+x_c] \end{aligned} \tag{16}$$

$$\begin{aligned} n_1(x,t) =& -\tfrac{\exp[-t(1+\gamma_{10})](\exp[t(1+\gamma_{10})]+\gamma_{10})(-1+H[x-x_c])}{x_c(1+\gamma_{10})}\\ &+\left\{-\tfrac{1}{x_c(1+\gamma_{10})}\exp[-(t-x)-t\gamma_{10}](\exp[(t-x)(1+\gamma_{10})]\right.\\ &+\gamma_{10})\\ &+\int_0^{t-x}-\tfrac{1}{x_c(1+\gamma_{10})}\exp[-(t-x-\tau)-(t-\tau)\gamma_{10}]\\ &\times(\exp[(t-x-\tau)(1+\gamma_{10})]+\gamma_{10})\\ &\left.\times\exp[-\tau]\tfrac{\sqrt{x\gamma_{10}}}{\sqrt{\tau}}I_1[2\sqrt{\tau x\gamma_{10}}]d\tau\right\}H[t-x]\\ &+\left\{\tfrac{1}{x_c(1+\gamma_{10})}\exp[(-x+x_c)\gamma_{10}-(t-x+x_c)(1+\gamma_{10})]\right.\\ &\times(\exp[(t-x+x_c)(1+\gamma_{10})]+\gamma_{10})\\ &+\int_0^{t-x+x_c}\tfrac{1}{x_c(1+\gamma_{10})}\exp[(-x+x_c)\gamma_{10}-(t-x+x_c-\tau)\\ &\times(1+\gamma_{10})](\exp[(t-x+x_c-\tau)(1+\gamma_{10})]+\gamma_{10})\\ &\left.\times\exp[-\tau]\tfrac{\sqrt{(x-x_c)\gamma_{10}}}{\sqrt{\tau}}I_1[2\sqrt{\tau(x-x_c)\gamma_{10}}]d\tau\right\}\\ &\times H[t-x+x_c]H[x-x_c] \end{aligned} \tag{17}$$

where $I_1(\eta)$ is the modified Bessel function of the first kind of order 1.

3. Results for a constant kinesin velocity

In order to convert solutions (16), (17) back to the dimensional form, the following substitutions are used:

$$\begin{aligned} &n_0^*=\frac{n_0\gamma_{01}^*}{v^*},\quad n_1^*=\frac{n_1\gamma_{01}^*}{v^*},\quad t^*=\frac{t}{\gamma_{01}^*}\\ &x^*=\frac{xv^*}{\gamma_{01}^*},\quad x_c=\frac{x_cv^*}{\gamma_{01}^*},\quad \gamma_{10}^*=\gamma_{10}\gamma_{01}^*. \end{aligned} \tag{18}$$

For the rat superior cervical ganglion neuron, Jung and Brown [23] reported the following values: $\gamma_{01}^*=0.041\,s^{-1}$, $\gamma_{10}^*=0.093\,s^{-1}$, and $v^*=0.55$ μm/s. The velocity value is slightly modified to $v^*=0.5644$ μm/s in order to match the expected value of kinesin velocity distribution (see Section 4). In addition, three values of the width of the initial pulse are used, $x_c^*=500, 750$, and 1000 μm. The above values are used in computing Figs. 2–5.

It is assumed that at $t^*=0$ all CEs are in the running state, and their concentration is $1/x_c^*$ (so that $\int_0^{x_c^*}n_1^*(x^*,0)dx^*=1$). Kinetic processes quickly redistribute CEs between the pausing and running states, until equilibrium concentrations are reached. The equilibrium concentrations are $n_{0eq}^*=\frac{\gamma_{10}}{(1+\gamma_{10})x_c^*}$ and $n_{1eq}^*=\frac{1}{(1+\gamma_{10})x_c^*}$ for the pausing and running states, respectively. For $x_c^*=0.5$ mm the equilibrium concentrations are 1.39 and 0.61 mm^{-1} for the pausing and running CEs, respectively;

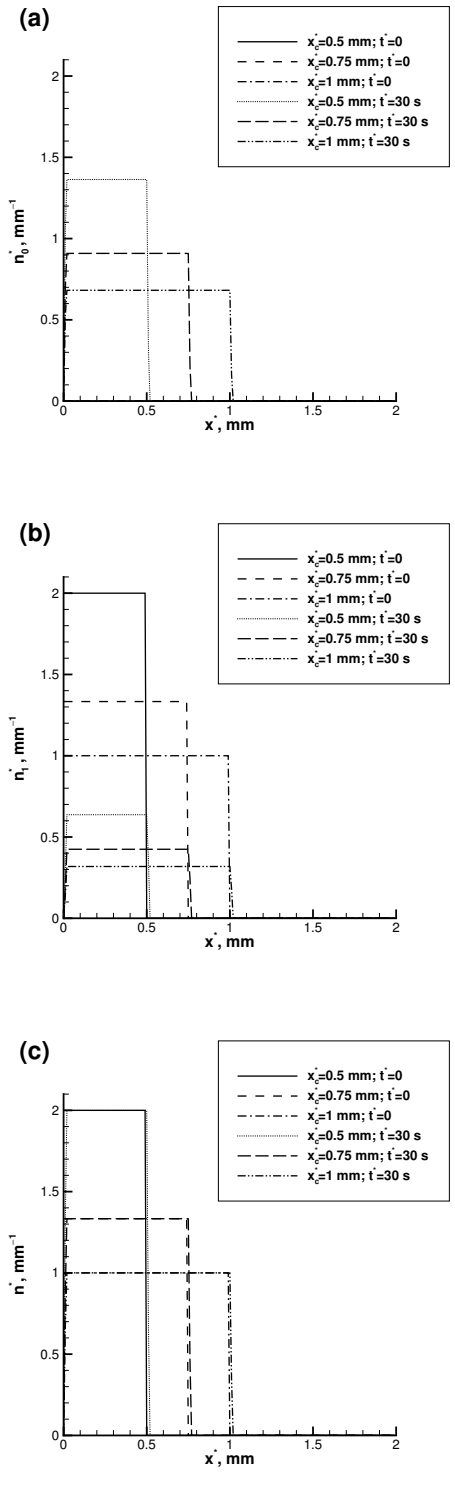

Figure 2. The case of constant kinesin motor velocity, $v^* = 0.5644$ μm/s. (a) Linear number density of pausing CEs, (b) Linear number density of running CEs, (c) Total linear number density of CEs (pausing and running). $\gamma_{01}^* = 0.041$ s^{-1}, $\gamma_{10}^* = 0.093$ s^{-1}, $t^* = 0$ and 30 s.

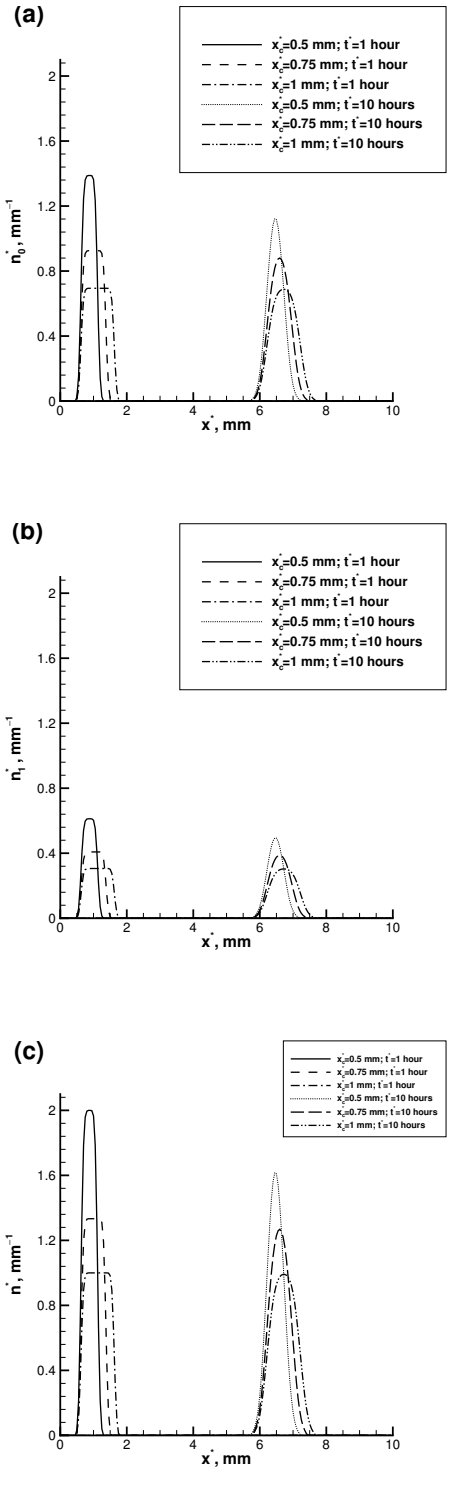

Figure 3. The case of constant kinesin motor velocity, $v^* = 0.5644$ μm/s. (a) Linear number density of pausing CEs, (b) Linear number density of running CEs, (c) Total linear number density of CEs (pausing and running). $\gamma_{01}^* = 0.041$ s^{-1}, $\gamma_{10}^* = 0.093$ s^{-1}, $t^* = 1$ hour (3.6×10^3 s) and 10 hours (3.6×10^4 s).

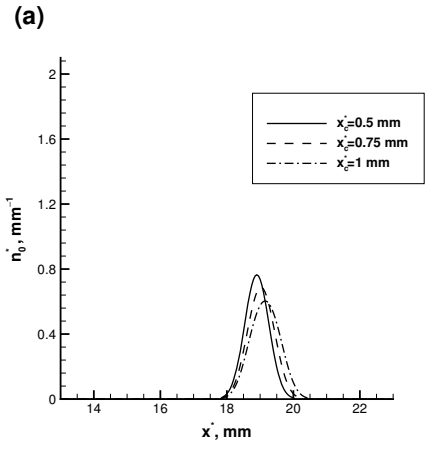

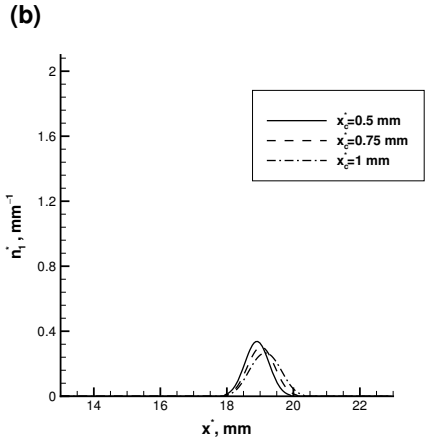

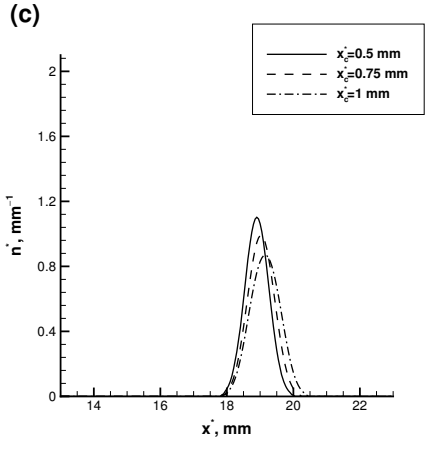

Figure 4. The case of constant kinesin motor velocity, $v^* = 0.5644$ μm/s. (a) Linear number density of pausing CEs, (b) Linear number density of running CEs, (c) Total linear number density of CEs (pausing and running). $\gamma_{01}^* = 0.041$ s^{-1}, $\gamma_{10}^* = 0.093$ s^{-1}, $t^* = 30$ hours (1.08×10^5 s).

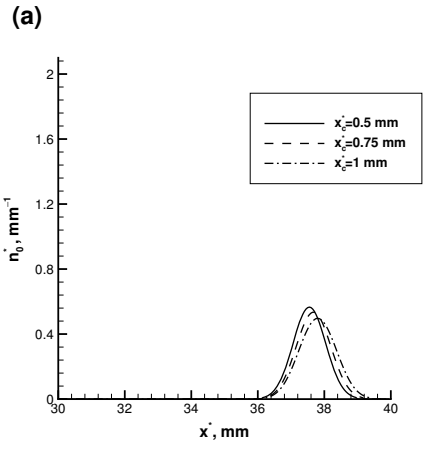

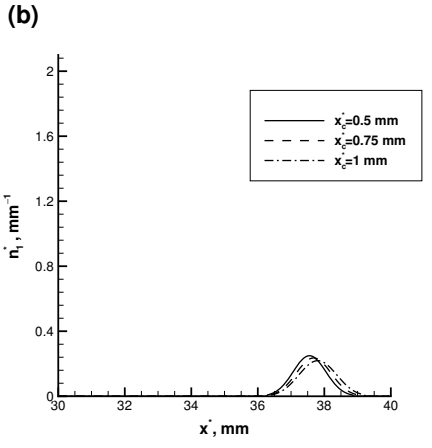

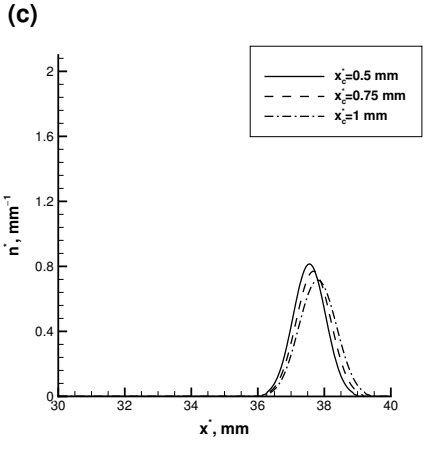

Figure 5. The case of constant kinesin motor velocity, $v^* = 0.5644$ μm/s. (a) Linear number density of pausing CEs, (b) Linear number density of running CEs, (c) Total linear number density of CEs (pausing and running). $\gamma_{01}^* = 0.041$ s^{-1}, $\gamma_{10}^* = 0.093$ s^{-1}, $t^* = 60$ hours (2.16×10^5 s).

for $x_c^* = 0.75$ mm these are 0.93 and 0.41 mm^{-1}, respectively, and for $x_c^* = 1$ mm these are 0.69 and 0.31 mm^{-1}, respectively. Fig. 2 shows that within the first 30 s the equilibrium concentrations are attained. It should be noted that during the initial stage of the process the concentration of running CEs uniformly decreases (from its value of $1/x_c^*$ at $t^* = 0$) and the concentration of pausing CEs uniformly increases (from its zero value at $t^* = 0$), but both concentrations retain the rectangular shape of the initial pulse displayed in Fig. 1 (c).

Fig. 3 shows the concentration waves at $t^* = 1$ and 10 hours. It is evident that by $t^* = 1$ hour the transition of concentration waves from rectangular pulses to bell-shaped waves has began. By $t^* = 10$ hours the bell-shaped waves typical for slow axonal transport [23] have formed. It is interesting that the waves corresponding to a larger width of the initial pulse, x_c^*, are slightly ahead of the waves corresponding to a smaller value of x_c^*. This is explained by the fact that for a larger value of x_c^* the geometric center of the initial pulse is slightly ahead of that for a smaller value of x_c^* (see Fig. 2), and this shift remains as the wave propagates.

Fig. 4 shows the concentration waves at $t^* = 30$ hours and Fig. 5 shows these at $t^* = 60$ hours. One can see that as the waves propagate, their amplitude decreases and the waves spread out; however, the probability of finding a CE in the axon (represented by $\int_0^\infty n^*(x^*, t^*)dx^*$) is equal to 1 at any t^*.

A comparison of concentration profiles displayed in Figs. 2–5 with experimentally measured profiles for NFs displayed in Fig. 6 of Jung and Brown [23] (these profiles are based on experimental data reported in [33]) indicate that in the experiment the concentration profiles spread out faster. One possibility of obtaining a closer match between the experiment and modeling is accounting for a possible retrograde motion of CEs. Physically, the switch to retrograde motion can occur if a dynein motor takes over. Such models were developed in [23]; however, they include either four or six kinetic states and therefore they are too complicated to obtain an analytical solution. Another possibility is accounting for the fact that all kinesin motors do not move with the same velocity, but rather exhibit a velocity distribution.

4. Effect of kinesin velocity distribution

The PDF of kinesin velocity distribution is found by fitting the experimental data reported in Fig. 2 (a) of Courty et al. [36] (Mathematica 8.0® FindFit operator is utilized):

$$f(v^*) = a v^* \exp\left[-\left(\frac{v^* + b}{c}\right)^2\right], \qquad (19)$$

where $a = 3535.6 s^2/\mu m^2$, $b = 3.9491 \mu m/s$, $c = 1.6388 \mu m/s$, the velocity of kinesin motors must be given in $\mu m/s$ and $f(v^*)$ is measured in $s/\mu m$. The expected velocity of the kinesin motor in this case is $E(v^*) = 0.5644 \mu m/s$ and the standard deviation is $\sigma(v^*) = 0.3708 \mu m/s$. The obtained PDF is displayed in Fig. 6.

Eqs. (16) and (17) (after Eq. (18) is used to convert them to the dimensional form) give concentrations of pausing and running CEs under the assumption that all CEs move with one and the same velocity v^*. The situation of when the kinesin velocity distribution is characterized by a PDF $f(v^*)$ can be approached as follows. Imagine that CEs and kinesin motors are characterized by color, depending on the velocity of the kinesin motor that transports a CE; green CEs are transported only by green kinesin motors that move with velocity v_1^*, red CEs are transported only by red kinesin motors that move with velocity v_2^*, etc. It is assumed that CEs do not switch the type of kinesin motors (even after a CE transitions to the pausing state and then back to the running state, it is moved by a kinesin motor of the same color). Physically this can be explained as follows. Imagine that transition to the pausing state occurs not due to kinesin motor detachment from a CE, but due to its deactivation. Transition back to the running state can then be interpreted as activation of the attached kinesin motor. Now consider the following situation at $t^* = 0$. Assume that initially the concentration of green CEs is $\kappa n_1^*(0, x^*)$ and the concentration of red CEs is $(1-\kappa)n_1^*(0, x^*)$, where $\kappa < 1$. If one is color-blind and wishes to know concentrations of CEs of any color (either green or red), one needs to calculate the sums with respect to different velocities, that is $\kappa n_0^*(x^*, t^*; v_1^*) + (1-\kappa)n_0^*(x^*, t^*; v_2^*)$ to obtain the concentration of pausing CEs and $\kappa n_1^*(x^*, t^*; v_1^*) + (1-\kappa)n_1^*(x^*, t^*; v_2^*)$ to obtain the concentration of running CEs [37]. Now let one have a large number of colors, and assume that the concentrations of these colored CEs at $t^* = 0$ are distributed according to a stepwise version of $f(v^*)$. Physically one can imagine that CEs from the initial pulse are picked up by kinesin motors whose velocity distribution is characterized by a PDF $f(v^*)$. In the limit of the infinite number of colors the concentrations of pausing and running CEs are given by the following integrals that express superpositions of concentrations corresponding to different kinesin velocities:

$$n_{0,f(v)}^*(x^*, t^*) = \int_0^\infty n_0^*(x^*, t^*; v^*) f(v^*) dv^* \qquad (20)$$

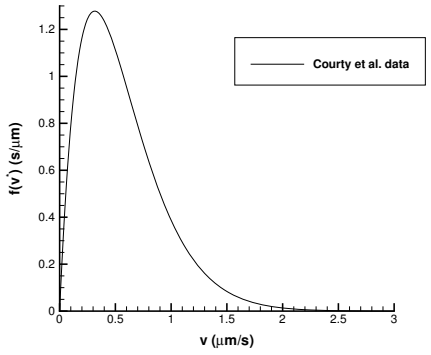

Figure 6. A PDF of kinesin velocity distribution based on data reported in Courty et al. [36]

$$n^*_{1,f(v)}(x^*, t^*) = \int_0^\infty n^*_1(x^*, t^*; v^*) f(v^*) dv^* . \qquad (21)$$

In practice the integrals on the right-hand sides of Eqs. (20) and (21) need to be calculated only over the interval of v^* where $f(v^*)$ is non-zero (see Fig. 6). If v^* is a constant (all kinesin motors move with one and the same velocity v^*_0) then $f(v^*) = \delta(v^* - v^*_0)$, where δ is a Dirac delta function.

Figs. 7 and 8 are computed for $\gamma^*_{01} = 0.041$ s^{-1}, $\gamma^*_{10} = 0.093$ s^{-1}, and $x^*_c = 1000$ μm. Fig. 7 compares concentration waves computed assuming a constant kinesin velocity (equal to the expected value of kinesin velocity distribution displayed in Fig. 6) and those computed using a PDF of the kinesin velocity. Wave profiles are presented for $t^* = 1$ and 5 hours. One can see that the CE concentration profiles start to deviate sharply between constant and distributed kinesin velocity situations after approximately 1 hour. Fig. 8 is similar to Fig. 7, but is computed for larger times, $t^* = 7$ and 10 hours. It is evident that in the case of a constant kinesin velocity the waves decay and spread out slowly while for the case of a distributed kinesin velocity the waves decay and spread out much faster.

It is interesting that although the shape of the wave is affected quite strongly by accounting for the kinesin velocity distribution, the velocity of the wave, defined as $\overline{v^*} = \frac{d}{dt^*}\int_0^\infty x^* n^*(x^*, t^*) dx^*$, is independent of whether the kinesin velocity is assumed constant or distributed. This property follows from the linearity of the problem (this fact has been also checked numerically); the velocity of the wave in either case remains constant and equal to $v^* \frac{\gamma^*_{01}}{\gamma^*_{01}+\gamma^*_{10}}$.

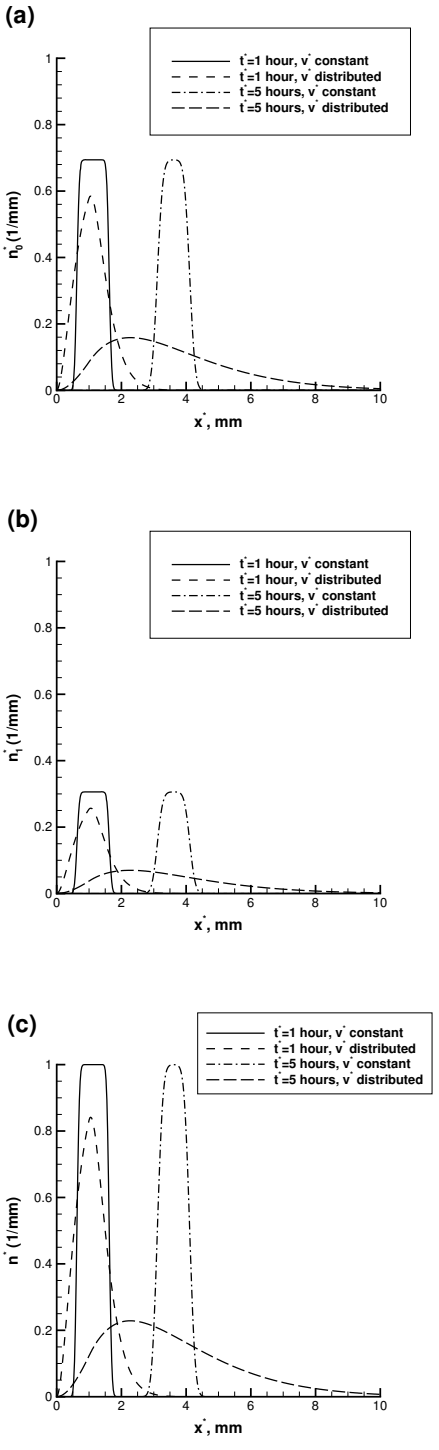

Figure 7. Comparison of CE waves for the cases when all CEs move with the same (expected) velocity and when there is a distribution of kinesin velocities. The average kinesin velocity is calculated as the expected value of the kinesin velocity distribution. (a) Linear number density of pausing CEs, (b) Linear number density of running CEs, (c) Linear number density of all (pausing and running) CEs in the axon. $\gamma^*_{01} = 0.041$ s^{-1}, $\gamma^*_{10} = 0.093$ s^{-1}, $x_c = 1$ mm, $t^* = 1$ hour (3.6×10^3 s) and 5 hours (1.8×10^4 s).

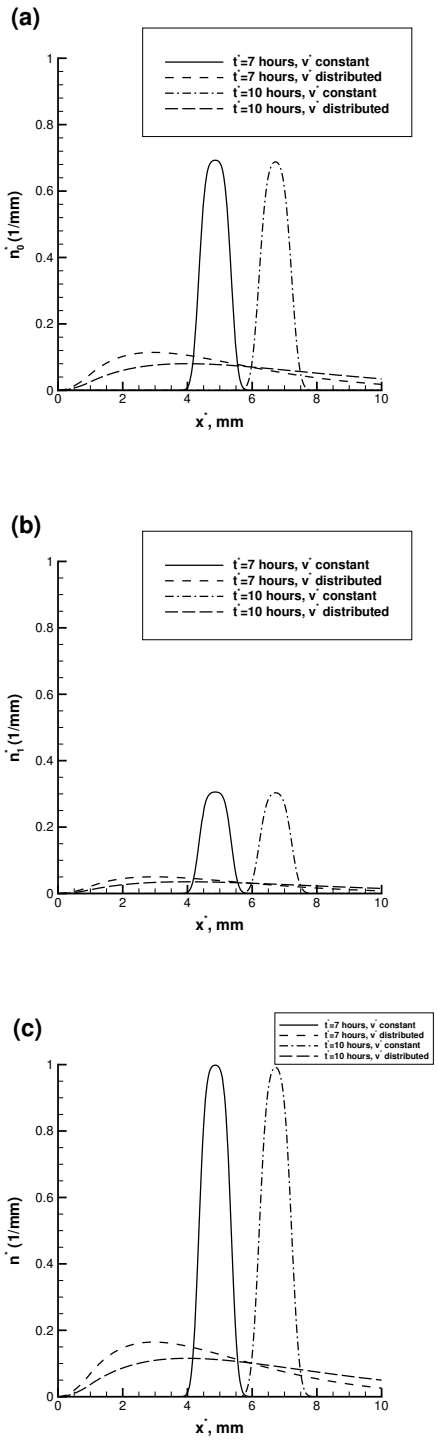

Figure 8. Comparison of CE waves for the cases when all CEs move with the same (expected) velocity and when there is a distribution of kinesin velocities. The average kinesin velocity is calculated as the expected value of the kinesin velocity distribution. (a) Linear number density of pausing CEs, (b) Linear number density of running CEs, (c) Linear number density of all (pausing and running) CEs in the axon. $\gamma_{01}^* = 0.041\ \mathrm{s}^{-1}$, $\gamma_{10}^* = 0.093\ \mathrm{s}^{-1}$, $x_c = 1$ mm, $t^* = 7$ hour (2.52×10^4 s) and 10 hours (3.6×10^4 s).

5. Conclusions

Utilizing the Laplace transform, the exact solution for the two kinetic state model simulating slow axonal transport based on the stop-and-go hypothesis is obtained. The obtained solution describes the concentrations of pausing and kinesin-driven CEs. Using this solution, the situations of constant and distributed kinesin velocity are studied. At the initial stage of the process, which takes less than one minute, kinetic processes redistribute CEs between pausing and running states. After that CE transport continues under conditions of kinetic equilibrium.

Based on published experimental data, an analytical curve-fit for a PDF characterizing the kinesin velocity distribution is obtained. In the beginning, there is not much difference between the constant and distributed kinesin velocity situations, but after approximately one hour the CE concentrations computed for these two cases start to deviate sharply. Accounting for the kinesin velocity distribution results in a faster decay of the concentration wave amplitude and faster spreading of the wave. However, the velocity of the wave is shown to be independent of whether the kinesin velocity is assumed constant or distributed.

References

[1] J.R. Fallon, A.B. Taylor, Protein Synthesis in Neurons, Encyclopedia of Life Sciences (Wiley, Hoboken, NJ, 2005)
[2] B. Alberts et al., Molecular Biology of the Cell, 5th ed. (Garland Science, New York, 2008)
[3] L.S.B. Goldstein, Z.H. Yang, Annu. Rev. Neuroscience 23, 39 (2000)
[4] S. Ally et al., J. Cell Biol. 187, 1071 (2009)
[5] P.E. Gallant, J. Neurocytology 29, 779 (2000)
[6] S.P. Gross, Phys. Biol. 1, R1 (2004)
[7] A.D. Pilling, D. Horiuchi, C.M. Lively, W.M. Saxton, Molec. Biol. Cell 17, 2057 (2006)
[8] M.A. Welte, Curr. Biol. 14, R525 (2004)
[9] J.V. Shah, D.W. Cleveland, Curr. Opinion Cell Biol. 14, 58 (2002)
[10] R.B. Vallee, G.S. Bloom, Annu. Rev. Neuroscience 14, 59 (1991)
[11] S. Roy et al., J. Neuroscience 27, 3131 (2007)
[12] J.T. Yabe, A. Pimenta, T.B. Shea, J. Cell Sci. 112, 3799 (1999)
[13] J.T. Yabe, C.W. Jung, W.K.H. Chan, T.B. Shea, Cell Motility and the Cytoskeleton 45, 249 (2000)
[14] J.V. Shah, L.A. Flanagan, P.A. Janmey, J.F. Leterrier, Molec. Biol. Cell 11, 3495 (2000)
[15] C.H. Xia et al., J. Cell Biol. 161, 55 (2003)

[16] P.W. Baas, D.W. Buster, J. Neurobiology 58, 3 (2004)
[17] S. Roy et al., J. Neuroscience 28, 5248 (2008)
[18] S. Terada et al., EMBO Journal 29, 843 (2010)
[19] A. Brown, L. Wang, P. Jung, Molec. Biol. Cell 16, 4243 (2005)
[20] A. Craciun, A. Brown, A. Friedman, J. Theor. Biol. 237, 316 (2005)
[21] A. Brown, Nat. Rev. Molec. Cell Biol. 1, 153 (2000)
[22] N. Trivedi, P. Jung, A. Brown, J. Neuroscience 27, 507 (2007)
[23] P. Jung, A. Brown, Phys. Biol. 6, 046002 (2009)
[24] A.V. Kuznetsov, A.A. Avramenko, D.G. Blinov, Int. J. Num. Meth. Biomed. Eng. 27, 1040 (2011)
[25] A.V. Kuznetsov, A.A. Avramenko, D.G. Blinov, J. Mechan. Med. Biol. 10, 445 (2010)
[26] A.V. Kuznetsov, A.A. Avramenko, D.G. Blinov, Int. Commun. Heat Mass Trans. 37, 770 (2010)
[27] A.V. Kuznetsov, A.A. Avramenko, D.G. Blinov, Int. Commun. Heat Mass Trans. 36, 641 (2009)
[28] A.V. Kuznetsov, A.A. Avramenko, D.G. Blinov, Int. Commun. Heat Mass Trans. 36, 293 (2009)
[29] A.V. Kuznetsov, A.A. Avramenko, D.G. Blinov, Cent. Eur. J. Phys. 9, 898 (2011)
[30] A.V. Kuznetsov, Cent. Eur. J. Phys. 9, 662 (2011)
[31] A.V. Kuznetsov, Comp. Methods Biomechanics Biomedical Eng., (2012), DOI: 10.1080/10255842.2012.662679, in press
[32] A.V. Kuznetsov, Proceedings of the Royal Society A, DOI: 10.1098/rspa.2012.0061, in press (2011)
[33] Z. Xu, V. Tung, Brain Res. 866, 326 (2000)
[34] H.S. Carslaw, J.C. Jaeger, Conduction of Heat in Solids, 2nd ed. (Clarendon press, Oxford, 1959)
[35] M. Abramowitz, I.A. Stegun (Eds.), Handbook of Mathematical Functions (Dover Publications, Mineola, NY, 1965)
[36] S. Courty et al., Nano Let. 6, 1491 (2006)
[37] A.V. Kuznetsov, Comp. Meth. Biomechanics Biomedical Eng., (2011), DOI: 10.1080/10255842.2011.632376, in press